TOPICAL REVIEW • OPEN ACCESS

Germanene: the germanium analogue of graphene

To cite this article: A Acun *et al* 2015 *J. Phys.: Condens. Matter* **27** 443002

OPEN ACCESS
IOP Publishing
Journal of Physics: Condensed Matter
J. Phys.: Condens. Matter **27** (2015) 443002 (11pp)
doi:10.1088/0953-8984/27/44/443002

Topical Review

Germanene: the germanium analogue of graphene

A Acun[1,6], L Zhang[1,6], P Bampoulis[1], M Farmanbar[2], A van Houselt[1], A N Rudenko[3], M Lingenfelder[4,5], G Brocks[2], B Poelsema[1], M I Katsnelson[3] and H J W Zandvliet[1]

[1] Physics of Interfaces and Nanomaterials, MESA$^+$ Institute for Nanotechnology, University of Twente, PO Box 217, 7500AE, Enschede, The Netherlands
[2] Computational Materials Science, MESA$^+$ Institute for Nanotechnology, University of Twente, PO Box 217, 7500AE, Enschede, The Netherlands
[3] Radboud University, Institute for Molecules and Materials, Heijendaalseweg 135, 6525 AJ Nijmegen, The Netherlands
[4] Max Planck-EPFL Laboratory for Molecular Nanoscience, École Polytechnique Fédérale de Lausanne, CH-1015 Lausanne, Switzerland
[5] Institut de Physique de la Matière Condensée, École Polytechnique Fédérale de Lausanne, CH-1015 Lausanne, Switzerland

E-mail: a.acun@utwente.nl

Received 8 May 2015, revised 7 August 2015
Accepted for publication 1 September 2015
Published 14 October 2015

Abstract

Recently, several research groups have reported the growth of germanene, a new member of the graphene family. Germanene is in many aspects very similar to graphene, but in contrast to the planar graphene lattice, the germanene honeycomb lattice is buckled and composed of two vertically displaced sub-lattices. Density functional theory calculations have revealed that free-standing germanene is a 2D Dirac fermion system, i.e. the electrons behave as massless relativistic particles that are described by the Dirac equation, which is the relativistic variant of the Schrödinger equation. Germanene is a very appealing 2D material. The spin-orbit gap in germanene (~24 meV) is much larger than in graphene (<0.05 meV), which makes germanene the ideal candidate to exhibit the quantum spin Hall effect at experimentally accessible temperatures. Additionally, the germanene lattice offers the possibility to open a band gap via for instance an externally applied electrical field, adsorption of foreign atoms or coupling with a substrate. This opening of the band gap paves the way to the realization of germanene based field-effect devices. In this topical review we will (1) address the various methods to synthesize germanene (2) provide a brief overview of the key results that have been obtained by density functional theory calculations and (3) discuss the potential of germanene for future applications as well for fundamentally oriented studies.

Keywords: germanene, 2D materials, scanning tunneling microscopy

(Some figures may appear in colour only in the online journal)

[6] Both authors have contributed equally to the work.

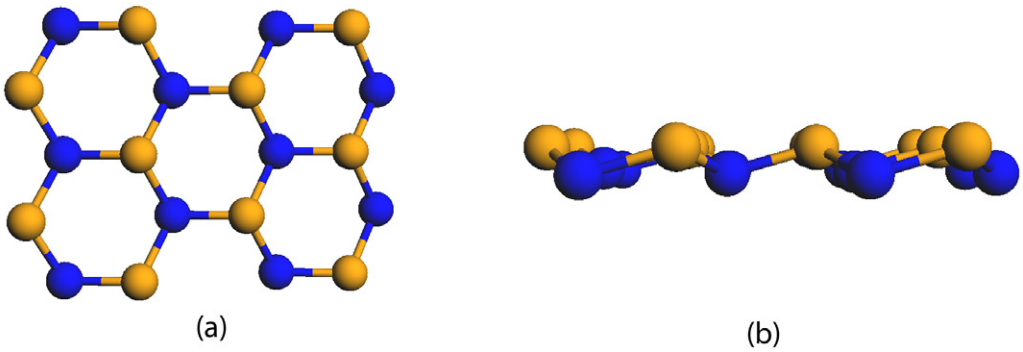

Figure 1. Ball and stick model of germanene. The honeycomb lattice is composed of two triangular sub-lattices (blue and brown atoms, respectively). Left panel: top view. Right panel: side view.

1. Introduction

The discovery of graphene, the first 2D material, has led to a cornucopia of new and exciting physics [1]. Graphene consists of sp^2 hybridized carbon atoms that are arranged in a planar configuration. The observation that a single free-standing sheet of atoms is stable was already quite a surprise, since the Mermin and Wagner theorem [2] states that a 2D crystal cannot exhibit long-range order at any finite temperature. In 1987 Nelson and Peliti [3] performed a theoretical study on the intricate interplay between crystalline order and thermal fluctuations in crystalline membranes. They showed that the anharmonic coupling between in-plane and out-of-plane (flexural) lattice vibrations is of crucial importance for the stability of a membrane, without this anharmonic coupling the membrane would be fully crumpled. As a result of this anharmonic coupling, the membrane becomes overall more or less flat, but the membrane displays strong intrinsic corrugations (ripples) that are characterized by a power-law behaviour of the atomic-displacement correlations functions. The system remains *approximately* 2D (with typical out-of-plane displacements that are much smaller than the sample size) and *approximately* crystalline (with a crystalline order which is preserved at finite, but very large distances) [4–6]. At least for rigid systems, such as graphene, this means that one can safely use the term '2D crystal' for any practical purpose [5]. Experimental studies have revealed that freely suspended graphene is indeed rippled [7].

The impressive rise of graphene has spurred many scientists to look for alternative 2D materials. The exploration of this new realm of 2D materials has barely begun, its promises have not yet fully materialized, and the extent of its potential for new physics and devices remains largely unexploited. The most obvious alternatives for graphene are the group IV elements, i.e. silicon and germanium [8–9]. The electron configurations of germanium, silicon and carbon are very similar since all three elements have four electrons in their outermost *s* and *p* orbitals. The energetically most favourable crystal structure of silicon and germanium is the diamond structure [10]. The diamond lattice consists of two interpenetrating *fcc* sub-lattices and each atom of these *fcc* sub-lattices is surrounded by four neighbours. The covalent bonds between the atoms are all equivalent and have a hybridized s, p_x, p_y, p_z character (sp^3). For carbon, another allotrope is found in nature that consists of a stack of sheets with a honeycomb structure (graphene). This carbon allotrope is named graphite and is under normal conditions, i.e. room temperature and atmospheric pressure, thermodynamically more stable than the carbon allotrope that has the diamond structure [11]. The three in-plane covalent bonds of graphene make angles of 120° with each other and have a hybridized $2s$, $2p_x$ and $2p_y$ character (sp^2). $2p_z$ electrons are itinerant and distributed throughout the whole carbon sheet, making the system metallic. These $2p_z$ orbitals give rise to the formation of the π bonding and π^* antibonding orbitals, which are largely responsible for the van der Waals interaction between the graphene sheets in graphite. For silicon and germanium such graphite-like allotropes have not been found in nature and therefore the silicon and germanium 'graphite' allotropes, hereafter referred as silicene and germanene respectively, are appealing candidates for synthesis.

Germanene, silicene and graphene share several very peculiar and interesting electronic properties. The electrons near the K and K' points of the Brillouin zone behave as relativistic massless particles. The electronic states of graphene near the Dirac points are described by a linear dispersion relation with a Fermi velocity of about 10^6 m s^{-1}. Already in the first experimental studies charge carrier mobilities as high as 15 000 cm^2 (V s)$^{-1}$ have been obtained [1]. Another hallmark of these 2D Dirac materials is that they display an anomalous ('half-integer') quantum Hall effect, which we will briefly touch upon in section 4. There are, however, also a few differences between germanene and silicence on the one hand and graphene on the other hand. Firstly, the honeycomb lattice of graphene is fully planar, whereas the honeycomb lattices of germanene and silicene are predicted to be buckled [12–14] (see figure 1). Secondly, due to the larger atomic number of germanium and silicon as compared to carbon, these materials have a much stronger spin–orbit coupling. A small buckling will increase the spin–orbit coupling by orders of magnitude [5]. The spin–orbit coupling results in the opening of a small band gap at the Dirac points in the interior of the material, topological protected gapless helical modes at the edges of the 2D material and a quantum spin Hall effect which is characterized by spin current transport via the edges modes [15, 16]. The spin–orbit gap in graphene, silicene and germanene are $<$0.05 meV, 1.55

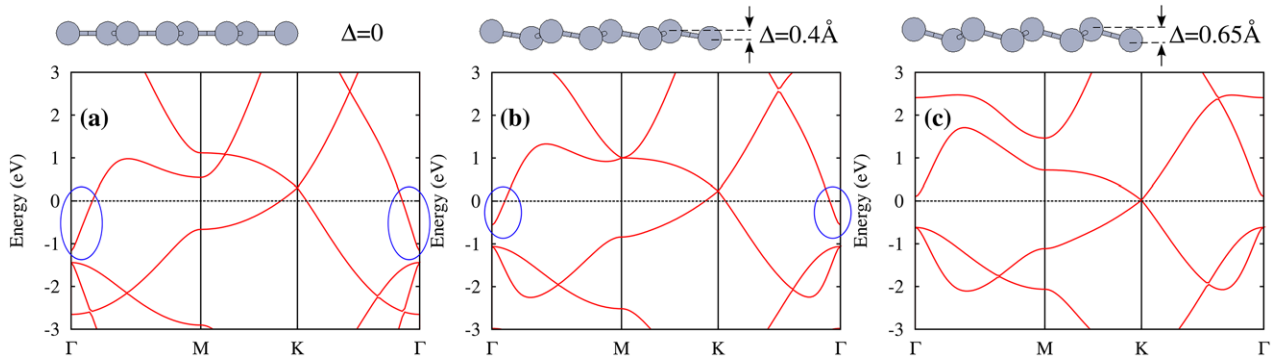

Figure 2. Electronic band structure of germanene calculated using DFT for different values of the buckling Δ. Zero energy corresponds to the Fermi energy. Blue circles denote the antibonding band crossing the Fermi energy at low buckling values.

meV and 23.9 meV, respectively [17–21]. This means that the quantum spin Hall state is only experimentally accessible for silicene and germanene [22, 23].

The first reports on the synthesis of silicene date back to 2010 [24–29], followed by germanene in 2014 [30–33]. Meanwhile silicene has been grown on several substrates (Ag(1 1 0), Ag(1 1 1), ZrB_2(0 0 0 1) and Ir(1 1 1)) and characterized by a variety of surface science techniques [24–29, 34]. Since there are already several reviews on silicene [35–37], we will restrict ourselves here to germanene. It is important to point out here that there are, besides graphene, silicene and germanene, a few more theoretically predicted 2D Dirac materials, such as stanene (Sn), *d*-wave superconductors (YBCO, LSCO), and transition metal-oxides as $(VO_2)_n/(TiO_2)$ [38]. In the last few years we have seen a flood of articles on other types of 2D materials such as phosphorene, arsenene, transition metal(di)chalcogenides (i.e. MoS_2, GaSe, WSe_2, WTe_2), organic crystals and artificial 2D lattices [38].

In this topical review we will attempt to give an update on the current status of germanene. We will start with a brief theoretical section where also density functional theory calculations of free-standing single-layer and bilayer germanene are presented. In section 3 the various methods to synthesize germanene will be presented and discussed. Subsequently we will present a section that discusses the peculiar electronic properties of germanene. We will elaborate on how the quantum spin Hall effect can be measured and how a substantial band gap can be opened in germanene. The review ends with a brief outlook that touches upon several technical issues that need to be solved before germanene-based electronic components come within reach.

2. Theoretical calculations

The first quantum mechanical *ab initio* calculations on 'graphite-like' silicon and germanium sheets were performed by Takeda and Shiraishi [12]. They found that the configuration with the lowest energy is buckled, i.e. the two sub-lattices of the honeycomb lattice are slightly displaced with respect to each other in a direction normal to the sheet. The *ab initio* calculations of Takeda and Shiraishi also revealed that silicene and germanene are semi-metals. Although these authors did not explicitly discuss the *k*-dependence of the electronic states that are responsible for the semi metallic character, it is clear from their energy band structure calculations that the dispersion relations are linear in *k*. In a later tight binding calculation Guzmán-Verri and Lew Yan Voon [13] pointed out that silicene has Dirac cones at the *K* and *K′* points of the Brillouin zone. These Dirac cones are robust against the buckling of the silicene lattice and therefore free-standing silicene is a 2D Dirac fermion system. A few years later Cahangirov *et al* [14] arrived at a similar conclusion for germanene and also demonstrated its structural stability with respect to atomic vibrations.

Since the theoretical prediction of stable free-standing germanene [14], its electronic and structural properties have been extensively studied by means of density functional theory (DFT) calculations [14, 39–45]. The calculations that are presented here are performed using the projected augmented wave (PAW) method [46] within the generalized gradient approximation (GGA) [47] as implemented in the VASP package [48, 49]. In comparison to graphene, the (π/π^*)-bonding in germanene is significantly weaker [40]. Apart from the increased interatomic distance, this results in a smaller energy splitting between the bonding and antibonding orbitals having significant consequences for the structure of germanene. Specifically, as can be deduced from the band structure of planar germanene (figure 2(a)), the low lying antibonding bands are partially occupied in the vicinity of the Γ-point, resulting in a finite density of states at the Fermi level. Being unfavourable from an energetic point of view, such states tend to be unoccupied, which is achieved in free-standing germanene by forming a buckled structure (figure 2(c)) at the expense of lowering the point group symmetry from D_{6h} to D_{3d} [41]. The buckling Δ, that is the vertical separation between the two sub-lattices, is ultimately determined by a balance between the electronic and elastic energies. For free-standing germanene, DFT studies report Δ in the range of 0.64–0.74 Å [44], depending on the computational scheme. Although configurations with a considerably larger buckling (>2 Å) also appear at the total energy landscape [12, 42], they do not seem to be realistic in view of the presence of imaginary modes in the phonon spectrum, implying dynamical instability of the corresponding structures. The buckling of germanene plays a crucial role in the formation of its intrinsic electronic properties. Particularly, the non-planar geometry along with a strong

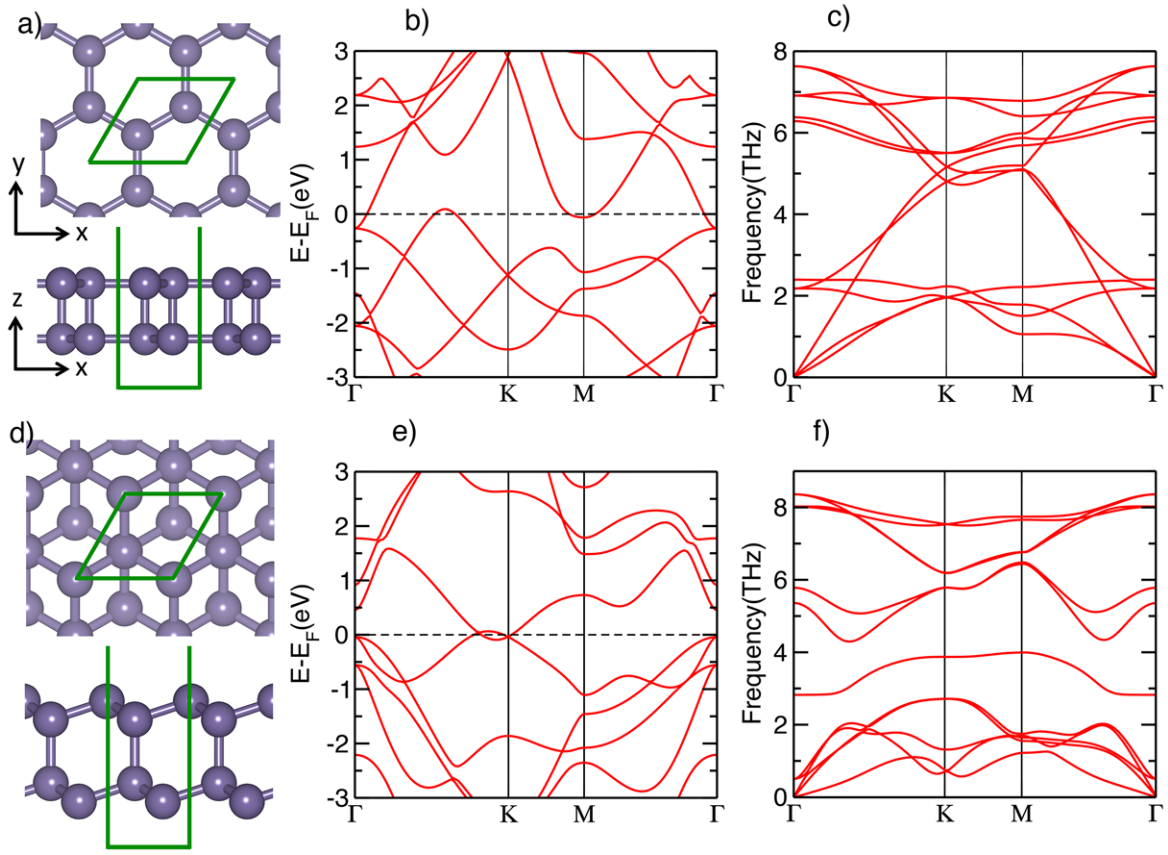

Figure 3. Top: (a) top and side view of the optimized AA-stacked structure of bilayer germanene (DFT calculation using the PBE/GGA functional); the optimized in-plane lattice constant is 4.43 Å. (b) the electronic bands along specific high symmetry directions in the 2D Brillouin zone; the zero of energy is at the Fermi level. (c) the phonon dispersions along the same directions. Bottom: (d) top and side view of the optimized AB-stacked structure of bilayer germanene; the optimized in-plane lattice constant is 4.08 Å. (e) the electronic bands and (f) the phonon dispersions of the AB-stacked structure.

spin–orbit interaction in germanene facilitates the opening of a considerable band gap at the Dirac point of the order of the thermal energy at room temperature (~24 meV) [20, 44].

The structural and electronic properties of germanene can be significantly modified by interactions with the underlying substrate [44, 45]. One mechanism that has been proven to be relevant for the magnitude of the buckling is lateral strain [39, 43], appearing for deposited structures due to improper matching between the lattice constants of the substrate and adsorbed layer. Similar to graphene, sub-lattice symmetry in supported germanene is generally not preserved, resulting in the opening of a band gap [44, 45].

Group IV element analogues of few-layer graphene, bilayer graphene in particular, have been studied theoretically and experimentally. Specifically bilayer silicene has been explored in quite some detail. DFT calculations of free-standing bilayer silicene predict several (meta)stable structures, where the two silicene layers are either in an AA or AB stacking [50–52]. Calculations of free-standing bilayer germanene give two similar, locally stable, optimized structures, with an AA-stacked structure (see top panels of figure 3) that is ~23 meV/atom more stable than an AB-stacked structure (see bottom panels of figure 3). The two Ge layers in the AA structure are planar, whereas in the AB structure they are buckled, reflecting an sp^2- and sp^3-type bonding in the AA and AB structures, respectively. The sp^2 bonding in the AA structure does not give rise to a strong intra-layer π-bonding like in bilayer graphene, however. In bilayer graphene the intra-layer bonding is strong, and the interlayer bonding originates from a weak, van der Waals interaction. In contrast, in AA bilayer germanene the intra- and interlayer interactions are of comparable strength. This is reflected in the structure, where both the intra- and the interlayer Ge–Ge bonds have a bond length of 2.56 Å. In the AB structure the intra- and interlayer Ge–Ge bonds have bond lengths of 2.49 Å, respectively 2.68 Å, which indicates that also in this structure intra- and interlayer interactions are comparable.

The strong interlayer bonding in bilayer germanene yields an electronic structure that is very different from that of bilayer graphene. In the bilayer germanene AA structure band minima at Γ and at M can be found close to the Fermi level, whereas the band maxima are located at Γ and ~0.6 ΓK, respectively (see figure 3(b)). The AB structure shows band minima at ~0.9 ΓK, and band maxima at Γ and ~0.9 ΓK close to the Fermi level, respectively (see figure 3(e)). DFT calculations with a conventional functional (PBE) based upon the generalized gradient approximation (GGA) [47], yield a semimetal for both structures. It is conceivable that a gap will be opened if a more advanced approach, such as *GW* [53, 54], is used to calculate the spectrum. The local stability of both

the AA and AB structures is demonstrated by the corresponding phonon spectra, in particular by the absence of any modes with an imaginary frequency, see figures 3(c) and (f). In bi- and multilayer graphene the weak interlayer bonding gives rise to low frequency optical modes [55]. The absence of any such modes in bilayer germanene is consistent with a strong interlayer bonding.

Whether adsorption of germanene or bilayer graphene on a substrate preserves the free-standing structures obviously depends on the interaction with the substrate. Adsorption of graphene, or its insulating counterpart, hexagonal boron nitride (*h*-BN), on metal surfaces ranges from weak physisorption to strong chemisorption, depending on the substrate [56–61]. The perturbation of the (electronic) structure of graphene then increases with increasing graphene-substrate interaction. Silicene is generally more reactive than graphene. The substrate-adsorbent interaction in silicene on Ag(1 1 1), for instance, is considerable, and although the adsorption preserves the hexagonal structure of silicene, the Ag substrate induces a sizable out-of-plane buckling of the Si atoms [62]. Hybridization between the silicene and the Ag states then leads to a large perturbation of the silicene electronic structure. Given the similarities between silicene and germanene, it is reasonable to assume that germanene behaves more like silicene than like graphene, when adsorbed on a metal substrate. Various structural models have been proposed to describe the existing experiments on germanene [30–33], see the next section. Their reliability has however not been unequivocally established. It is, for instance, worth noting that the honeycomb structures observed in the STM experiments on Au-Ge and Pt-Ge [30–32] can also be attributed to the hexagonal (1 1 1) surfaces of Ge_2Pt or Ge_2Au *fcc* crystals, where the honeycomb termination only might be visible in experiments due to the unequal electronic density in the vicinity of Ge and Pt (Au) atoms and also due to the symmetry-governed vertical displacement of surface atoms.

3. Synthesis of germanene

The synthesis of germanene and germanene-related materials was initiated by a report by Bianco *et al* [63] on the preparation and exfoliation of germanane (GeH). Germanane, i.e. hydrogen terminated germanene, was successfully prepared via the topochemical deintercalation of $CaGe_2$. Germanane sheets can be obtained by simple exfoliation of the layered van der Waals solid. At ambient conditions germanane is very stable and only oxidizes in a time span of several months. This stability is an important prerequisite for the usage of germanane in any technological application. The strong potential of germanane for technological applications is fueled by theoretical calculations, which predict a direct band gap of 1.5 eV and an electron mobility that is substantially higher than that of bulk germanium [64, 65].

As pointed out in the preceding section free-standing germanene is stable against local lattice distortions. To date germanene has been reported to be synthesized on only a few substrates. In July 2014 Li *et al* [30] reported the growth of germanene on Pt(1 1 1). Germanium was deposited on a pristine Pt(1 1 1) substrate at room temperature under ultra-high vacuum conditions from a germanium rod mounted in an electron-beam evaporator. After deposition the Pt substrate was annealed at a temperature in the range of 600–750 K for 30 min. Using low energy electron diffraction and scanning tunneling microscopy they found a $(\sqrt{19} \times \sqrt{19})$ periodicity with respect to the Pt(1 1 1) substrate. Their scanning tunneling microscopy data revealed the presence of a continuous and well-ordered $(\sqrt{19} \times \sqrt{19})$ superstructure, which they interpreted as a germanene adlayer on the Pt(1 1 1) substrate. Unfortunately, Li *et al* [30] did not manage to obtain atomic resolution. Line scans recorded with a scanning tunneling microscope showed that the $(\sqrt{19} \times \sqrt{19})$ superstructure has a corrugation of about 0.6 Å. The authors ascribed this corrugation to Ge atoms that are located at different positions on the Pt(1 1 1) substrate. A density functional theory calculation revealed that the $(\sqrt{19} \times \sqrt{19})$ superstructure coincides with a germanene layer that has a (3×3) periodicity (see figure 4(A)). Recently, Švec *et al* [66] suggested that the $(\sqrt{19} \times \sqrt{19})$ reconstruction on Pt(1 1 1) is actually not germanene, but a surface alloy composed of Ge_3Pt tetramers that resembles a twisted kagome lattice. These authors based their conclusion on a comprehensive study of the closely related Si/Pt(1 1 1) system.

The second paper on the synthesis of germanene is by Davila *et al* [31]. They reported the growth of germanene on Au(1 1 1). These authors performed a combined scanning tunneling microscopy and low energy electron diffraction study and they identified three different phases: a $(\sqrt{7} \times \sqrt{7})R19.1°$ phase, a (5×5) phase and a $(\sqrt{19} \times \sqrt{19})R23.4°$ phase (all referred to the periodicity of the Au(1 1 1) substrate). The $(\sqrt{7} \times \sqrt{7})$ phase (also referred as the $(\sqrt{3} \times \sqrt{3}$ phase) exhibits a nearly flat honeycomb structure. Based on these observations Davila *et al* ascribed the $(\sqrt{7} \times \sqrt{7})$ phase to germanene (see figure 4(B)). Their conclusion is supported by synchroton radiation core-level spectroscopy measurements and density functional theory calculations.

A few days after the appearance of Davila's publication another paper appeared by Bampoulis *et al* [32], where the formation of germanene terminated Ge_2Pt clusters was reported. Bampoulis *et al* deposited a few monolayers Pt on a Ge(1 1 0) substrate and subsequently annealed the sample at 1100 K. The bulk phase diagram of Pt-Ge system exhibits an eutectic at 1043 K. This occurs at a composition of 22% and 78% Pt and Ge, respectively. Low energy electron microscopy (LEEM) images revealed that slightly above this eutectic temperature liquid drops are formed and move as large entities across the surface [32]. Interestingly, for the other low-index surfaces of germanium an eutectic top-layer is formed, rather than droplets. [67–70]. This difference is due to the relatively high surface free energy of Ge(1 1 0) as compared to the Ge(0 0 1) and Ge(1 1 1) surfaces [71, 72]. Upon cooling down the eutectic $Pt_{0.22}Ge_{0.78}$ droplets that have been formed on the Ge(1 1 0) surface they solidify and spinodal decomposition occurs. The eutectic phase separates in a pure Ge phase and Ge_2Pt phase, respectively. The phase with the lowest surface free energy, i.e. Ge, segregates towards to the surface of the droplet, whereas the interior is composed of the

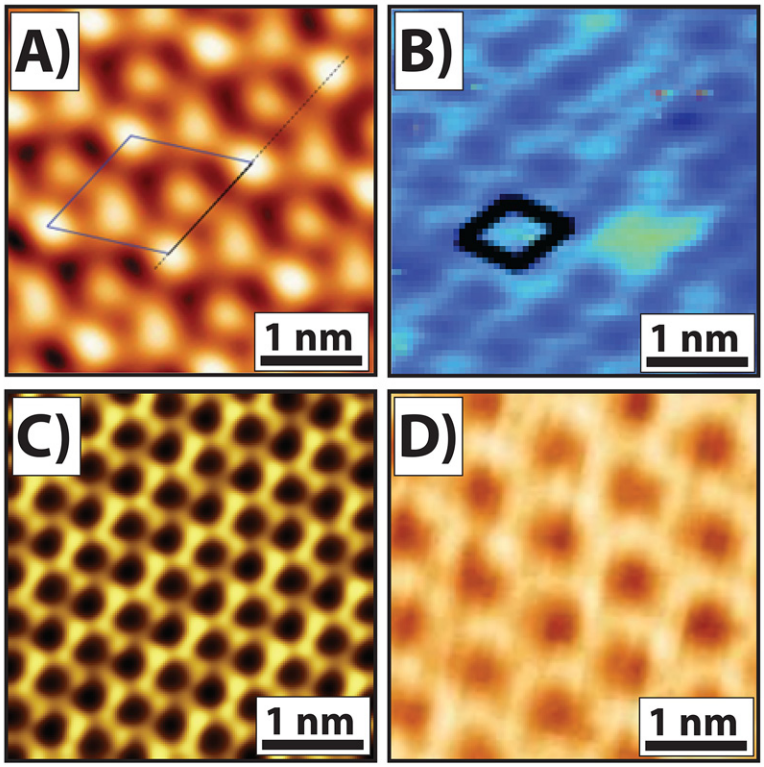

Figure 4. STM images of germanene sheets grown by several research groups. For comparison all the images have the same size of 4 nm × 4 nm. (A) STM image of the germanene $\sqrt{19} \times \sqrt{19}$ superstructure on Pt(1 1 1). ($V = 1$ V and $I = 0.05$ nA), [30] (B) STM image of the germanene $\sqrt{3} \times \sqrt{3}$ superstructure on Au(1 1 1) ($V = -1.12$ V and $I = 1.58$ nA; the Au(1 1 1) $\sqrt{7} \times \sqrt{7}$ unit cell is outlined in black), [31] (C) STM image of the germanene honeycomb layer on a Ge_2Pt cluster ($V = -0.5$ V and $I = 0.2$ nA), [32] and (D) STM image of the germanene 3 × 3 superstructure on Al(1 1 1) ($V = -0.7$ V and $I = 0.3$nA), [33]. Printed with permission. Image courtesy of Wiley [30], Institute of Physics [31, 32] and the American Chemical Society [33].

other phase, i.e. the Ge_2Pt alloy. After solidification the surface of the droplets exhibit a buckled honeycomb structure. Scanning tunneling microscopy images reveal and atomically resolved buckled honeycomb lattice with a nearest-neighbor distance of 2.5 ± 0.1 Å (see figure 4(C)). Bampoulis *et al* [32] also found that the honeycomb lattice is buckled and composed of two triangular sub-lattices, which are displaced with respect to each other by only 0.2 Å. This buckling is much smaller than the 0.65 Å that is reported in several density functional theory calculations for free-standing germanene. As has been shown above free-standing germanene is metallic for buckling values smaller than about 0.6 Å. The scanning tunneling spectra reported by Bampoulis *et al* [32] revealed a metallic-like behavior. Two remarks are in place here (1) it is very well possible that the electronic states of the germanene top layer hybridizes with the underlying substrate and (2) the recorded scanning tunneling spectra are also affected by the electronic structure of the scanning tunneling microscope tip.

The recent most paper on the growth of germanene is by Deviraz *et al* [33] and appeared in 2015. These authors found a (3 × 3) (referred to the Al(1 1 1) surface) reconstruction on Al(1 1 1) which they ascribed to germanene (see figure 4(D)). The (3 × 3) reconstruction forms a continuous layer that covers the Al(1 1 1) and has domain sizes of 100 nm, or larger. Density functional theory calculations showed that the unit cell consists of eight Ge atoms. The observed buckling is due to the fact that two out of the eight atoms of the (3 × 3) unit cell are displaced upwards. The low energy electron diffraction and scanning tunneling microscopy observations are in agreement with their density functional theory calculations.

Although the experimental studies have revealed honeycomb-like reconstructions [30–33] it remains to be seen if the grown germanene indeed behaves as a 2D Dirac fermion system. Angle-resolved photoemission experiments are needed to reveal if the synthesized germanene sheets indeed have Dirac cones at the *K* points of the surface Brillouin zone. Another test would be to apply a magnetic field normal to the germanene sheet and measure the Landau levels with for instance scanning tunneling microscopy [73]. The presence and separation of the Landau levels will immediately reveal whether one deals with a 2D electron gas or a 2D Dirac fermion system.

To date germanene has only been grown on metallic substrates. It is very likely that the relevant electronic states of germanene near the Fermi level hybridize with electronic states of the metallic substrate and destroy the 2D Dirac character of the germanene. It would be a huge step forward if germanene could be synthesized on a wide band gap material. A possible candidate would be hexagonal boron nitride (*h*-BN). *h*-BN has a band gap of about 6 eV and its lattice constant (2.5 Å) is almost identical to the nearest neighbor distance of germanene (see figure 5).

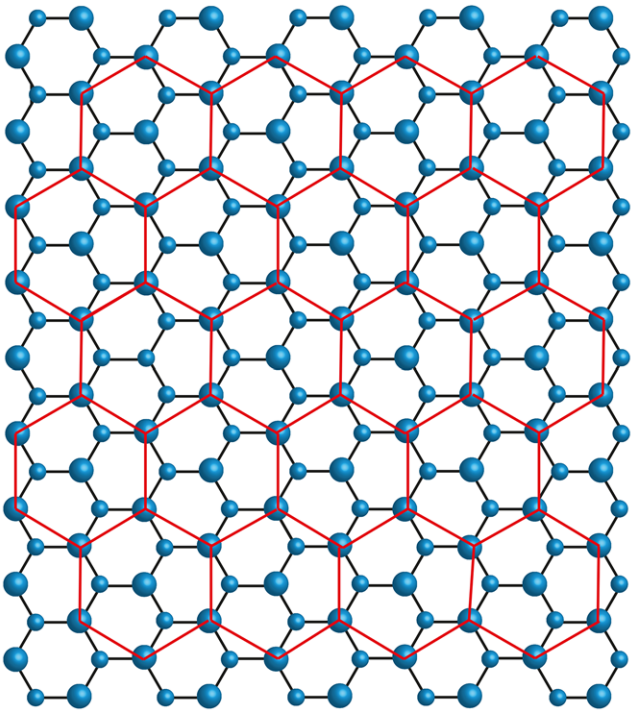

Figure 5. Germanene sheet (red honeycomb) on a *h*-BN substrate (blue honeycomb). The nearest-neighbour distance of germanene and the lattice constant of *h*-BN are both 2.5 Å.

4. Outlook: the future of germanene

4.1. Anomalous quantum Hall effect

The electrons in the vicinity of the Dirac points in free-standing germanene are described by the relativistic variant of the Schrödinger equation, the Dirac equation [6, 74–77]. A standard tight binding calculation reveals that there are two conical bands at the K and K' points of the Brillouin zone, respectively. The dispersion relation is linear, i.e. $E = v_F\hbar k$, where v_F is the Fermi velocity and $\hbar$ the reduced Planck constant. The Dirac cones lead to a zero density of states at the Fermi level and a linear in energy density of states away from the Fermi level. The peculiar electronic structure of 2D Dirac materials leads to a number of intriguing physical properties. As already pointed out in the introduction the anomalous quantum Hall effect is one of these intriguing properties. For a conventional 2D electron gas the Landau levels are equidistant and the separation between consecutive levels is given by $\hbar\omega_c$, where $\omega_c = eB/m$ is the cyclotron frequency with B a magnetic field normal to the 2D system. For a 2D Dirac system, however, the energy spectrum is given by $\pm v_F\sqrt{n\hbar eBn}$ ($n = 0$, 1, 2, …). Importantly, zero-energy Landau level ($n = 0$) exists which is topologically protected with respect to possible inhomogeneity of magnetic field (or pseudomagnetic field created by deformations) [6]. Since this level is equally shared by electrons and holes the Hall conductivity per channel turns out to be half-integer (in the units of e^2/h) instead of normal integer quantization. This anomalous quantum Hall effect is one of the most powerful tests to check whether a 2D material is indeed a Dirac fermion system. There is yet another intriguing aspect that needs to be mentioned namely the Klein paradox [6]. A quantum mechanical particle with energy E has a non-zero probability to overcome a potential barrier U that is larger than E (tunnelling). For nonrelativistic particles, the transmission probability decays exponentially with the height and the width of the barrier. In the case of 2D Dirac fermion materials, however, the transmission probability for electrons that incident normally is always equal to unity independent of the actual height and width of the barrier.

4.2. Quantum spin Hall effect

One of the most appealing properties of germanene is its large spin-orbit gap of about 24 meV. The latter implies that this 2D material is the ideal candidate for the observation of the quantum spin Hall effect (QSHE). The QSHE is of broad interest because of its scientific importance as a novel quantum state of matter and its potential for technological applications in the fields of spintronics, valleytronics and quantum computation.

In a conventional quantum Hall system the applied external magnetic field causes the electrons to move in well-defined circles. The electrons, which all orbit in the same clock (or anti-clock) wise direction, bounce back at the edges of the sample leading to a net flow of current along the edges of the sample. This current flows in one direction, and therefore, no back-scattering can occur resulting in a dissipation-less flow of charge. In contrast to the quantum Hall effect, the quantum spin Hall effect does not require an external magnetic field [15, 16]. The spin-orbit coupling leads to an internal magnetic field that couples to the spin of the electrons. This asymmetry will result into two spin-polarized conduction channels at the edges of the 2D material that propagate in opposite directions, the so-called gapless helical edge modes. The QSHE is therefore characterized by a vanishing charge Hall conductance and a quantized spin Hall conductance of $2e/4\pi$ (an electron with charge e carries a spin $\hbar/2$ and therefore the spin Hall conductance becomes $(2e^2/h) \cdot (\hbar/2e) = 2e/4\pi$).

The QSHE in 2D materials was first proposed by Kane and Mele for graphene in 2005 [15, 16], however due to the very small spin-orbit coupling in graphene extremely low temperatures are required for the realization of the QSHE state. In 2006 Bernevig, Hughes and Zhang predicted that the QSHE can also occur in CdTe/HgTe/CdTe quantum wells [78]. By varying the thickness of the quantum well, the band structure can be switched from a normal to an 'inverted' type at a critical thickness. Shortly after this prediction the QSHE state in a CdTe/HgTe/CdTe quantum well was experimentally confirmed by König *et al* [79]. These authors convincingly demonstrated at low-temperatures ($T < 1.4$ K) the presence of an edge conductance $2e^2/h$ that only exists beyond the critical layer thickness of the quantum well.

The spin-orbit coupling depends on the atomic number and therefore silicene and germanene, which exhibit spin-orbit gaps of 1.55 meV and 23.9 meV, respectively, are very attractive 2D materials regarding the possible observation of the QSHE. Germanene is particularly appealing because it would allow to observe the QSHE at temperatures near room temperature. The most straightforward test to check the presence of the topological protected edge modes, which is one of the

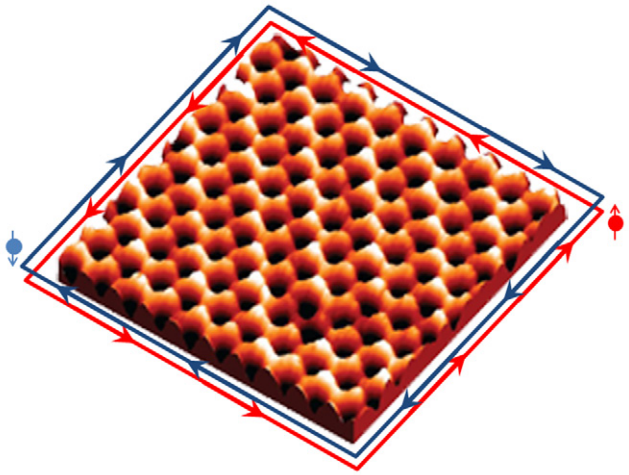

Figure 6. Schematic diagram of the quantum spin Hall effect for a 2D material. The quantum spin Hall effect is characterized by topological protected gapless helical edge modes that have a vanishing charge Hall conductance and a quantized spin Hall conductance.

hallmarks of the QSHE, is by making a spatial map of the differential conductivity at zero bias $((\mathrm{d}I/\mathrm{d}V)_{V=0})$. In the interior of the 2D topological insulator there will be a spin-orbit gap, whereas this gap closes at the edges of the 2D material. Spatial maps of the differential conductivity can be obtained by recording IV traces using scanning tunnelling microscopy with the feedback disabled. Alternatively the differential conductivity can be obtained directly by adding a small sinusoidal voltage to the sample bias and subsequently measure the differential conductivity using a lock in amplifier.

As discussed above the QSHE is characterized by a quantized spin Hall conductance and a vanishing charge Hall conductance. In the absence of an external bias the spin-up current that flows in one direction along the edges is fully cancelled by the spin-down current that flows in the opposite direction (see figure 6). The latter does not hold for the spin current, because spin-up and spin-down currents that flow in *opposite* directions add up and therefore the total spin conductance is $2e/4\pi$ [80]. Upon the application of an external bias the quasi Fermi levels of the left and right propagating spin-up and spin-down electrons are not equal anymore and this results into a net flow of electrons with conductance e^2/h. At the opposite edge the position of the quasi Fermi levels are reversed and therefore also here we have a net flow of electrons (now in the same direction) with conductance e^2/h. The total edge charge conductance in case of an applied bias is therefore $e^2/h + e^2/h = 2e^2/h$.

By using a multi-probe scanning tunneling microscope the edge conductance can be measured as a function of temperature as well as the number and separation of the probes. The separation between the probes should be smaller than the elastic mean free path of the charge carriers ($\lambda_{\mathrm{MFP}} \sim 1000\,\mathrm{nm}$ for a charge carrier mobility of $\sim 10^5\ \mathrm{cm}^2\ (\mathrm{V\ s})^{-1}$. It should be emphasized here that the number of probes could affect the transport measurement. A straightforward Landauer-Büttiker analysis reveals that the four-terminal conductance is given by $G_{14,23} = I_{14}/V_{23} = 2e^2/h$, whereas the two-terminal conductance is $G_{14,14} = I_{14}/V_{14} = 2e^2/3h$ [75]. The separate positioning of four scanning tunnelling microscope tips is far from trivial, however Baringhaus *et al* [81] recently demonstrated that the conductance of graphene nanoribbons can be measured using this method.

Recently, Seixas, Padilha and Fazzio [82] proposed that the QSHE might also be observed in germanene nanoroads embedded in a hydrogenated germanene (germanane) matrix. These nanoroads can be experimentally realized by local hydrogen dissociation of germanane.

4.3. Opening of a band gap in germanene

In order to open a band gap in germanene or silicene charge should be transferred from one sub-lattice to the other sub-lattice. Due to the buckling it is easier to open a band gap in germanene and silicene than in their planar counterpart graphene [83, 84]. The band gap at K and K' points of the Brillouin zone of germanene upon the application of an electric field with the voltage V in a direction normal to the germanene sheet is given by,

$$E_\sigma(k) = \pm\sqrt{(v_{\mathrm{F}}\hbar k)^2 + \left(\Delta_{\mathrm{SO}} + \frac{1}{2}\xi\sigma eV\right)^2} \qquad (1)$$

where $\sigma = \pm 1$ refers to the spin and $\xi = \pm 1$ to the K and K' points, respectively. Δ_{SO} denotes the spin-orbit coupling. From equation (1) it immediately follows that there are two branches, one with a band gap $\left|\Delta_{\mathrm{SO}} + \frac{1}{2}\xi eV\right|$ and another with a band gap $\left|\Delta_{\mathrm{SO}} - \frac{1}{2}\xi eV\right|$. At the critical field, i.e. $\Delta_{\mathrm{SO}} = \frac{1}{2}eV$, the smaller gap closes resulting in a transition from a topological insulator to a semi metal. For electric fields larger than the critical field germanene becomes a normal band insulator. Thus, upon increasing the electric field the gap of germanene first closes and then opens again (see figure 7 for a simple schematic diagram).

Besides the interesting topological aspects of the band gap opening in germanene it also opens the door to the realization of germanene based field-effect devices, such as for instance a transistor [85, 86]. One should realize that for a proper operation of such a germanene based field-effect transistor a band gap opening of at least 300–400 meV is required.

There are several ways to open a band gap in germanene via the transfer charge from one sub-lattice to the other. As has been shown in the preceding paragraph one way to realize this charge transfer is by applying an external electric field in a direction perpendicular to the germanene. For graphene the application of an electric field does not result into the opening of gap because graphene is completely flat and so the electric field only leads to a shift of the potential. For silicene Ezawa [87–90] and Drummond *et al* [91] have predicted that silicene undergoes an interesting topological phase transition as a function of the applied electrical field. In the absence of an electric field silicene is a Z_2 topological insulator. With increasing applied electric field the band gap first closes (at a critical electric field, E_{c}, of 20 meV $\mathrm{\AA}^{-1}$), and subsequently the gap opens again (the gap opening increases

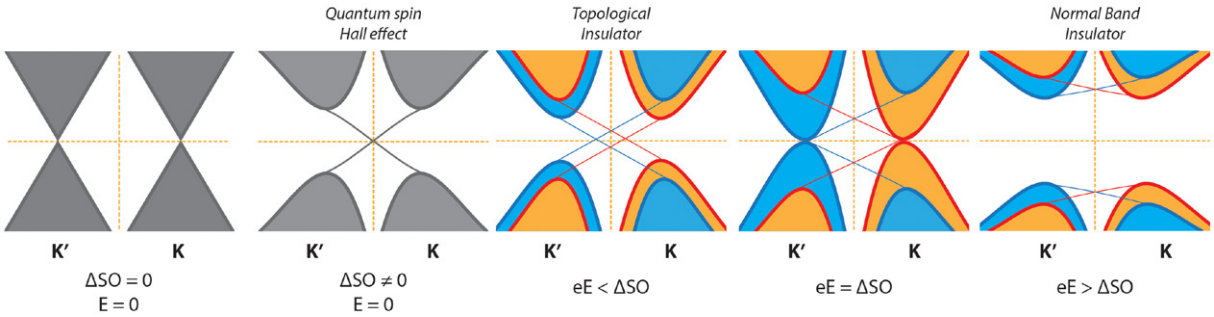

Figure 7. Schematic diagram of the effect of an external electric field on the electronic structure near the Dirac point. Dirac cones at the K and K′ points of the Brillouin zone.

linearly with applied electric field). At the critical electric field there is a gapless spin-up band at the K point of the Brillouin zone, whilst the spin-down band is gapless at the K' point of the Brillouin zone. For electric fields larger than E_c there are no gapless edge modes and thus we are dealing with a normal band insulator. For electric fields exceeding ~0.5 V Å^{-1} the calculations of Drummond *et al* [91] revealed that the conduction band at the Γ point and the valence band at the K point start to overlap leading to semi-metallic behavior of silicene. Given the similarity between silicene and germanene one expects a similar behavior for germanene, albeit the external applied electric field that is required to close the spin–orbit gap is larger for germanene [92].

One could also try to manipulate the charger transfer between the two sub-lattices via chemical ways, for instance via the adsorption or intercalation of foreign molecules or via coupling with a substrate [93]. The drawback of these chemical methods is, however, that the electronic band structure of germanene might be severely affected. In case one aims at field-effect applications of germanene it is not a problem that the Dirac nature of the material is lost, but it is much more important that the modification of the electronic structure does not lead to a severe degradation of the charge carrier mobilities. Another route to manipulate the electronic structure is to apply an external strain [94], possibly in combination with the application of an external electric field [95].

For silicene Quhe *et al* [96] have predicted that band gap openings as large as 0.5 eV can be realized via the adsorption of alkali atoms on one side of the silicene sheet. A band gap of 0.5 eV would result into an on/off ratio of 10^8, which meets the requirement for field-effect based applications. Using density functional theory calculations Ni *et al* [97] showed that a band gap in silicene can also be opened by the adsorption of metal atoms, such as Cu, Ag, Au, Ir and Pt. Some of these metals give rise to n-type doping (Cu, Ag and Au), whereas Ir results into p-type doping and Pt has hardly any effect on the doping level of the silicene. Ye *et al* [44] showed that a sizeable band gap in germanene can be realized by the adsorption of alkali metal atoms [98]. They claim that the band gap can be tuned from 0.02 eV to 0.31 eV by varying the coverage of adsorbed alkali atoms. The effective masses of the electrons and holes near the K and K' points of the Brillouin zone after the adsorption of alkali atoms are relatively small and therefore the carrier mobilities are expected to be affected only marginally. Since germanene has only just recently been synthesized experimental studies of the tuning of germanene's band gap that could test the abovementioned theoretical predictions are not yet available.

As a final remark we would like to mention that germanene nanoribbons also might have a band gap and therefore these nanoribbons can serve as the basis for a field-effect transistor [98]. However, in order to realize band gaps in germanene in the range of 0.3–0.5 eV the nanoribbons should have a width of only a few atoms, which renders this scenario very challenging from an experimental point of view. For germanene's counterpart, i.e. silicene, a number of possible scenarios to realize a silicene-based field-effect based transistor have already been put forward [99–102]. Early 2015 the realization of the first silicene transistor was reported by Tao *et al* [86]. Despite the fact that the lifetime of this silicene transistor was only a few minutes the achievements of Tao *et al* are impressive given the challenging experimental hurdles that they had to overcome.

5. Conclusions

In summary, germanene's debut has been impressive, but there are still many aspects that require further study. The first point of concern is to validate that the reported honeycomb lattices are indeed composed of germanium atoms. The second, and equally important, point of concern deals with the electronic structure of the germanene layers. To date there is no experimental evidence whatsoever that the germanene layers that have been synthesized so far are indeed 2D Dirac systems. Since it is of utmost importance to decouple the relevant electronic states of the germanene layer from the underlying substrate the most straightforward approach is to synthesize germanene on materials with a substantial band gap. Once it has experimentally been settled that the synthesized germanene is indeed a 2D Dirac material the door to several very intriguing and interesting experiments, such as the quantum spin Hall effect and the opening of the band gap of germanene, is opened [103].

Regarding the applicability of germanene in the microelectronic industry we envisage that for the realization of a germanene transistor the same hurdles need to be overcome as for a silicene transistor. For instance, the reactivity of germanene regarding oxygen and water as well as the interaction

of germanene with the substrate are expected to be very comparable to silicene. In order to protect these 2D materials to ambient conditions and electronic coupling with the substrate, encapsulating them with a wide band gap material, such as *h*-BN, Al_2O_3 [104] or AlN, is most probably the best solution. As already pointed out in section 3 *h*-BN, has a nearly perfect lattice match with germanene and is therefore a very appealing substrate for the growth of germanene. High quality single *h*-BN layers are nowadays routinely grown by thermally cracking of borazine $B_3H_6N_3$ on various metal substrates, such as Ir(1 1 1), Cu(1 1 1), Ni(1 1 1) and Rh(1 1 1) [105–110]. It remains however to be seen if the deposition of germanium on *h*-BN indeed leads to the formation of germanene.

With the current information at hand there are no major differences in the expected performance of silicene and germanene transistors. An advantage of germanene are the large intrinsic carrier mobilities, which are predicted to be a factor of 2–3 higher than the intrinsic carrier mobilities of silicene [21]. This difference is attributed to the weak coupling of charge carriers with in-plane phonons and the large buckling of germanene. A disadvantage of germanene is, however, that germanene is not as compatible with the current silicon-based microtechnology as silicene.

Acknowledgments

AA and PB thank the Nederlandse organisatie voor wetenschappelijk onderzoek (NWO) for financial support. HJWZ, MF and GB thank the Stichting voor Fundamenteel Onderzoek der Materie (FOM) for financial support. LZ thanks the China Scholarship Council for financial support. ANR and MIK acknowledge financial support by the European Union Seventh Framework Programme under Grant Agreement No. 604391 Graphene Flagship.

References

[1] Novoselov K S, Geim A K, Morozov S V, Jiang D, Zhang Y, Dubonos S V, Grigorieva I V and Firsov A A 2004 *Science* **306** 666
Geim A K and Novoselov K S 2007 *Nat. Mater.* **6** 183
[2] Mermin N D 1968 *Phys. Rev*. **176** 250
[3] Nelson D R and Peliti L 1987 *J. Physique* **48** 1085
[4] Fasolino A, Los J H and Katsnelson M I 2007 *Nat. Mater.* **6** 858
[5] Katsnelson M I and Fasolino A 2013 *Acc. Chem. Res.* **46** 97
[6] Katsnelson M I 2012 *Graphene: Carbon in Two Dimensions* (Cambridge: Cambridge University Press) Chapter 9
[7] Mozorov S V, Novoselov K S, Katsnelson M I, Schedin F, Ponomarenko L A, Jiang D and Geim A K 2006 *Phys. Rev. Lett*. **97** 016801
[8] Le Lay G, Salomon E, Angot T, Dávila M E 2015 *Micro- and Nanotechnology Sensors, Systems, and Applications VII* (*Proc. of SPIE* vol 9467) ed T George *et al* p 94670U-1
[9] Le Lay G, Salomon E, De Padova P, Layet J-M and Angot T 2014 *Aust. J. Chem*. **67** 1370–2
[10] Bundy F P 1964 *J. Chem. Phys.* **41** 3809
[11] Bundy F P 1989 *Physica* A **156** 169
[12] Takeda K and Shiraishi K 1994 *Phys. Rev.* B **50** 14916
[13] Guzmán-Verri G G and Lew Yan Voon L C 2007 *Phys. Rev.* B **76** 075131
[14] Cahangirov S, Topsakal M, Aktürk E, Şahin H and Ciraci S 2009 *Phys. Rev. Lett.* **102** 236804
[15] Kane C L and Mele E J 2005 *Phys. Rev. Lett*. **95** 146802
[16] Kane C L and Mele E J 2005 *Phys. Rev. Lett.* **95** 226801
[17] Boettger J C and Trickey S B 2007 *Phys. Rev.* B **75** 121402
[18] Gmitra M, Konschur S, Ertler C, Ambrosch-Draxl C and Fabian J 2009 *Phys. Rev.* B **80** 235431
[19] Abdelouahed S, Ernst A, Henk J, Maznichenko I V and Mertig I 2010 *Phys. Rev.* B **82** 125424
[20] Liu C-C, Feng W and Yao Y 2011 *Phys. Rev. Lett.* **107** 076802
[21] Ye X-S, Shao Z-G, Zhao H, Yang L and Wang C-L 2014 *RSC Adv.* **4** 21216
[22] Han W, Kawakami R K, Gmitra M and Fabian J 2014 *Nat. Nanotechnol.* **9** 794–807
[23] Konschuh S, Gmitra M and Fabian J 2010 *Phys. Rev.* B. **82** 245412
[24] Aufray B, Kara A, Vizzini S, Oughaddou H, Léandri C, Ealet B and Le Lay G 2010 *Appl. Phys. Lett*. **96** 183102
[25] De Padova P *et al* 2010 *Appl. Phys. Lett*. **96** 261905
[26] Le Lay G, De Padova P, Resta A, Bruhn T and Vogt P 2012 *J. Phys. D: Appl. Phys.* **45** 392001
[27] De Pavoda P, Quaresima C, Olivieri B, Perfetti P and Le Lay G 2011 *Appl. Phys. Lett*. **98** 081909
[28] Fleurence A, Friedlein R, Ozaki T, Kawai H, Wang Y, Yamada-Takamura Y 2012 *Phys. Rev. Lett*. **108** 245501
[29] Vogt P, De Padova P, Quaresima C, Frantzeskakis J A E, Asensio M C, Resta A, Ealet B and Le Lay G 2012 *Phys. Rev. Lett*. **108** 155501
[30] Li L, Lu S-Z, Pan J, Qin Z, Wang Y-Q, Wang Y, Cao G, Du S and Gao H-J 2014 *Adv. Mater*. **26** 4820
[31] Dávila M E, Xian L, Cahangirov S, Rubio A and Le Lay G 2014 *New J. Phys.* **16** 095002
[32] Bampoulis P, Zhang L, Safaei A, van Gastel R, Poelsema B and Zandvliet H J W 2014 *J. Phys.: Condens. Matter* **26** 442001
[33] Derivaz M, Dentel D, Stephan R, Hanf M-C, Mehdaoui A, Sonnet P and Pirri C 2015 *Nano Lett.* **15** 2510
[34] Acun A, Poelsema B, Zandvliet H J W and van Gastel R 2013 *Appl. Phys. Lett.* **103** 263119
[35] Kara A, Enriquez H, Seitsonen A P, Lew Yan Voon L C, Vizzini S, Aufray B, Oughaddou H 2012 *Surf. Sci. Rep*. **67** 1
[36] Yamada-Takamura Y and Friedlein R 2014 *Sci. Technol. Adv. Mater.* **15** 064404
[37] Lew Yan Voon L C and Guzman-Verri G G 2014 *MRS Bull.* **39** 366
[38] Wang J, Deng S, Liu Z and Liu Z 2015 *Natl Sci. Rev.* **2** 22–39
[39] Houssa M, Pourtois G, Afanasév V V and Stesmans A 2010 *Appl. Phys. Lett.* **96** 082111
[40] Roome N J and Carey J D 2014 *ACS Appl. Mater. Interfaces* **6** 7743
[41] Nijamudheen A, Bhattacharjee R, Choudhury S and Datta A 2015 *J. Phys. Chem.* C **119** 3802
[42] Trivedi S, Srivastava A and Kurchania R 2014 *J. Comput. Theor. Nanosci.* **11** 781
[43] Cai Y, Chuu C-P, Wei C M and Chou M Y 2013 *Phys. Rev.* B **88** 245408
[44] Ye M, Quhe R, Zheng J, Ni Z, Wang Y, Yuan Y, Tse G, Shi J, Gao Z and Lu J 2014 *Physica* E **59** 60
[45] Li X, Wu S, Zhou S and Zhu Z 2014 *Nanoscale Res. Lett.* **9** 110
[46] Blöchl P 1994 *Phys. Rev.* B **50** 17953
[47] Perdew J P, Burke K and Ernzerhof M 1996 *Phys. Rev. Lett.* **77** 3865
[48] Kresse G and Furthmüller J 1996 *Phys. Rev.* B **54** 11169
[49] Kresse G and Joubert J 1999 *Phys. Rev.* B **59** 1758

[50] Kamal C, Chakrabarti A, Banerjee A and Deb S K 2013 *J. Phys.: Condens. Matter* **25** 085508
[51] Liu H, Han N and Zhao J 2014 *J. Phys.: Condens. Matter* **26** 475303
[52] Huang B, Deng H-X, Lee H, Yoon M, Sumpter B G, Liu F, Smith S C and Wei S-H 2014 *Phys Rev. X* **4** 021029
[53] Hedin L 1965 *Phys. Rev.* **139** A796
[54] Shishkin M and Kresse G 2006 *Phys. Rev.* B **74** 035101
[55] Hazrati E, de Wijs G A and Brocks G 2014 *Phys. Rev.* B **90** 155448
[56] Giovannetti G, Khomyakov P A, Brocks G, Karpan V M, van den Brink J and Kelly P J 2008 *Phys. Rev. Lett.* **101** 026803
[57] Khomyakov P A, Giovannetti G, Rusu P C, Brocks G, van den Brink J and Kelly P J 2009 *Phys. Rev.* B **79** 195425
[58] Bokdam M, Brocks G, Katsnelson M I and Kelly P J 2014 *Phys. Rev.* B **90** 085415
[59] Mittendorfer F, Garhofer A, Redinger J, Klimeš J, Harl J and Kresse G 2011 *Phys. Rev.* B **84** 201401
[60] Rudenko A N, Keil F J, Katsnelson M I and Lichtenstein A I 2012 *Phys. Rev.* B **86** 075422
[61] Olsen T and Thygesen K 2013 *Phys. Rev.* B **87** 075111
[62] Pflugradt P, Matthes L and Bechstedt F 2014 *Phys Rev.* B **89** 205428
[63] Bianco E, Butler S, Jiang S, Restrepo O D, Windl W and Golberger J E 2013 *ACS Nano* **7** 4414
[64] Lew Yan Voon L C, Sandberg E, Aga R S and Farajin A A 2010 *Appl. Phys. Lett.* **97** 163114
[65] Houssa M, Scalise E, Sankaran K, Pourtois G, Afanasév V V and Stesmans A 2011 *Appl. Phys. Lett.* **98** 223107
[66] Švec M *et al* 2014 *Phys. Rev.* B **89** 201412
[67] Gurlu O, Adam O A O, Zandvliet H J W and Poelsema B 2003 *Appl. Phys. Lett.* **83** 4610
[68] Oncel N, van Houselt A, Huijben J, Hallbäck A-S, Gurlu O, Zandvliet H J W and Poelsema B 2005 *Phys. Rev. Lett.* **95** 116801
[69] Safaei A, Poelsema B, Zandvliet H J W and van Gastel R 2014 *New J. Phys.* **16** 113052
[70] Saedi A, Poelsema B and Zandvliet H J W 2011 *Surf. Sci.* **605** 507
[71] Bampoulis P, Acun A, Zhang L and Zandvliet H J W 2014 *Surf. Sci.* **626** 1
[72] Zandvliet H J W 2003 *Phys. Rep.* **388** 1
[73] Lin C-L, Arafune R, Kawahara K, Kanno M, Tsukahara N, Minamitani E, Kim Y, Kawai M and Takagi N 2013 *Phys. Rev. Lett.* **110** 076801
[74] Dirac P 1928 *Proc. R. Soc.* A **118** 610–7
[75] Wallace P R 1947 *Phys. Rev.* **71** 622–34
[76] Castro Neto A H, Guinea F, Peres N M R, Novoselov K S and Geim A K 2009 *Rev. Mod. Phys.* **81** 109–62
[77] Wehling T O, Black-Schaffer A M and Balatsky A V 2014 *Adv. Phys.* **63** 1
[78] Bernevig B A, Hughes T L and Zhang S-C 2006 *Science* **314** 1757
[79] König M, Wiedmann S, Brüne C, Roth A, Buhmann H, Molenkamp L W, Qi X-L and Zhang S-C 2007 *Science* **318** 766
[80] Hasan M Z and Kane C L 2010 *Rev. Mod. Phys.* **82** 3045
[81] Baringhaus J *et al* 2014 *Nature* **506** 349
[82] Seixas L, Padilha J E and Fazzio A 2014 *Phys. Rev.* B **89** 195403
[83] Jose D and Datta A 2012 *J. Phys. Chem.* C **116** 24639–48
[84] Ezawa M 2012 *New J. Phys.* **14** 033003
[85] Zandvliet H J W 2014 *Nano Today* **9** 691
[86] Tao L, Cinquanta E, Chiappe D, Grazianetti C, Fanciulli M, Dubey M, Molle A and Akinwande D 2015 *Nat. Nanotechnol.* **10** 227
[87] Ezawa M 2012 *New J. Phys.* **16** 065015
[88] Ezawa M 2013 *Eur. Phys. J.* B **86** 139
[89] Ezawa M 2012 *Phys. Rev. Lett.* **109** 055502
[90] Ezawa M 2013 *Phys. Rev. Lett.* **110** 026603
[91] Drummond N D, Z´olyomi V and Fal'ko V I 2012 *Phys. Rev.* B **85** 075423
[92] Kaloni T P, Modarresi M, Tahir M, Roknabadi M R, Schreckenbach G and Freund M S 2015 *J. Chem. Phys.* C **119** 11896
[93] Kaloni T P, Schreckenbach G and Freund M S 2014 *J. Phys. Chem.* C **118** 25200
[94] Kaloni T P and Schwingenschlögl U 2013 *Chem. Phys. Lett.* **583** 137
[95] Yan J A, Gao S-P, Stein R and Coard G 2015 *Phys. Rev.* B **91** 245401
[96] Quhe R *et al* 2012 *Sci. Rep.* **2** 853
[97] Ni Z, Zhong H, Jiang X, Quhe R, Luo G, Wang Y, Ye M, Yang J, Shi J and Lu J 2014 *Nanoscale* **6** 7609
[98] Xia W, Hu W, Li Z and Yang J 2014 *Phys. Chem. Chem. Phys.* **16** 22495
[99] Kaneko S, Tsuchiya H, Kamakura Y, Mori N and Ogawa M 2014 *Appl. Phys. Express* **7** 035102
[100] Li H, Wang L, Liu Q, Zheng J, Mei W-N, Gao Z, Shi J and Lu J 2012 *Eur. Phys. J.* B **85** 274
[101] Ezawa M 2013 *Appl. Phys. Lett.* **102** 172103
[102] Sadeghi H 2014 *J. Nanosci. Nanotechnol.* **14** 4178
[103] Zhang L, Bampoulis P, van Houselt A and Zandvliet H J W 2015 *Appl. Phys. Lett.* **107** 111605
[104] Molle A, Grazianetti C, Chiappe D, Cinquanta E, Cianci E, Tallarida G and Fanciulli M 2013 *Adv. Funct. Mat.* **23** 4340
[105] Auwärter W, Kreutz T J, Greber T and Osterwalder J 1999 *Surf. Sci.* **429** 229
[106] Corso M, Auwärter W, Muntwiler M, Tamai A, Greber T and Osterwalder J 2004 *Science* **303** 217
[107] Laskowski R, Blaha P, Gallauner T and Schwarz K 2007 *Phys. Rev. Lett.* **98** 106802
[108] Corso M, Greber T and Osterwalder J 2005 *Surf. Sci.* **577** L78
[109] Roth S, Matsui F, Greber T and Osterwalder J 2013 *Nano Lett.* **13** 2668
[110] Schulz F, Drost R, Hämäläinen S K, Demonchaux T, Seitsonen A P and Liljeroth P 2014 *Phys. Rev.* B **89** 235429